J Nanostruct 16(2): 2147-2160, Spring 2026

RESEARCH PAPER

Enhancing the Polymerization Properties of Plastics Using a Bio-Engineered Nanoscale Catalyst System

Muntaha Mahmoud Al-Rashidy [1], ***Mira Ausama Al-Katib*** [2], ***Mohanad Yakdhan Saleh*** [3] *

[1] *Nineveh Education Directorate, Iraqi Ministry of Education, Iraq*

[2] *Department of Biology, College of Education for pure Science, University of Mosul, Iraq*

[3] *Department of Chemistry, College of Education for pure Science, University of Mosul, Iraq*

ARTICLE INFO

Article History:
Received 25 December 2025
Accepted 14 February 2026
Published 01 April 2026

Keywords:
Charophyta
Choline chloride
Nanoparticles
Polycondensation

ABSTRACT

The green synthesis of nanomaterials using algae is an effective and sustainable approach for developing environmentally friendly chemical catalysts (ChCl-based DES/AgNPs catalyst). The algae *Chara vulgaris* was used to synthesize two different nanomaterials: silver nanoparticles (AgNPs) and iron oxide nanoparticles (Fe_2O_3 NPs), The catalytic efficiency in plastic polymers synthesis was evaluated .The nanoparticles were prepared using an aqueous extract of *Chara vulgaris* algae as a reducing agent, and the resulting materials were characterized using multiple techniques: UV-Visible spectroscopy, scanning electron microscopy (SEM) to study particle size and morphology, X-ray diffraction (XRD) to determine the crystalline structure of the particles, and FTIR spectroscopy to identify the functional groups responsible for the reduction process. The results showed the success of the nanoparticle preparation process through their color change and homogeneous distribution; the absorption spectrum of Fe_2O_3NPs (350 nm) and AgNPs (450 nm) According to scanning electron microscopy (SEM), the average size of iron nanoparticles (Fe_2O_3 NPs) was 52 nm, with sizes between from (20-100 nm), while the average size of silver nanoparticles (Ag NPs) was 41 nm, with sizes between from (20-90 nm), XRD revealed the crystalline nature of the particles, with iron particles exhibiting a hexagonal crystal system and the absence of any peaks attributable to impurities, whereas silver particles had face-centered cubic crystal structures. FTIR confirmed the presence of functional groups such as proteins, carbohydrates, phenols, and carbonyls. These particles were applied as heterogeneous catalysts in polymerization reactions, and the results demonstrated high catalyst efficiency in improving the properties of the resulting polymer and reducing reaction time compared to conventional catalysts used in polymer synthesis. This opens new horizons for the production of sustainable bioplastics at lower cost and with high.

How to cite this article
Mahmoud Al-Rashidy M., Ausama Al-Katib M., Yakdhan Saleh M. Enhancing the Polymerization Properties of Plastics Using a Bio-Engineered Nanoscale Catalyst System. J Nanostruct, 2026; 16(2):2147-2160. DOI: 10.22052/JNS.2026.02.060

* *Corresponding Author Email: mohanadalallaf@uomosul.edu.iq*

INTRODUCTION

Plastic waste is one of the most important problems globally due to its accumulation in the environment and its non-biodegradability, which causes plastic pollution. Therefore, an innovative solution to this pollution had to be found through bioplastics, a material that is environmentally friendly due to its low carbon footprint, sustainability, and low toxicity, in addition to its high degradation rate. It is a suitable alternative to plastics manufactured from fossil fuels [1-3]. In addition to plastic waste accumulation, environmental pollution caused by contaminants in water [4-6] and air [7-9] has become a major global concern. Industrial activities, agricultural runoff, fossil fuel combustion, and improper waste disposal release hazardous substances into aquatic and atmospheric environments, negatively affecting ecosystems and human health. Water pollution threatens aquatic organisms and reduces water quality, while air pollution contributes to respiratory diseases, climate change, and environmental degradation [5, 6]. Consequently, the development of sustainable and eco-friendly technologies has become essential to reduce pollution and promote environmental protection.

Interest in the biosynthesis of nanoparticles has emerged due to the significant risks associated with synthesizing them through physical and chemical methods, which lead to the production of toxic chemicals on the surface of the nanoparticles, in addition to their high manufacturing costs and the need for reducing agents, stabilizers, and strong reducing agents that pose health and environmental risks [10-17]. Recent advances in microfluidic technology have provided powerful tools for biological and biomedical research by enabling precise control of cellular microenvironments. These technologies offer significant advantages, including reduced reagent consumption, enhanced experimental reproducibility, and the ability to closely mimic physiological conditions [18-20].

To address these significant issues, the potential for green synthesis using plants and algae has been explored, as they contain a range of active compounds such as phenolic compounds, flavonoids, and glycosides, which can be used to synthesize nanoparticles more precisely and safely [21, 22]. This synthesis has achieved remarkable progress in terms of cost, ease of synthesis, environmental friendliness, and the fact that it does not require high heat, pressure, or energy [23].

Nanoparticles are characterized by their high stability and biocompatibility, with sizes ranging from 1 to 100 nanometers and various shapes, including spherical, cubic, triangular, rod-shaped, and others [24]. They possess novel chemical and physical properties, such as increased reaction rates, and exhibit magnetic and electrical properties that differ from those of the original material [25].

Algae of various types are effective tools in the synthesis of silver nanoparticles, such as blue-green algae [26] and green algae such as Ulva [27]. These algae are considered living factories, and *Chara vulgaris* is a safe source for their production [28]. *Chara* is characterized by its diverse forms and is found in many regions worldwide; it is a freshwater alga found in ponds and rivers [29] It is capable of environmental adaptation and treating heavy metal pollution such as arsenic [30] and is considered a promising bio-resource that opens new horizons for environmental sustainability.

MATERIALS AND METHODS

Sample Collection and Macroscopic Identification

The sample was collected from the Zammar region in Iraq. After confirming the sample's purity, the algae were identified macroscopically by preparing temporary slides of the sample and examining them under a light microscope at 40X magnification to determine the genus and species of the algae. It was then washed and cleaned of dust, dried in an oven at a temperature of 40-50°C for 3-4 days, ground using a porcelain mortar, and stored in tightly sealed containers until use.

Preparation of the hexane extract from the algae

After collection, drying, and grinding, a Soxhlet apparatus was used according to the method described by [31] to prepare the hexane extract, fifty grams of the powder were placed in a filter paper folded into a funnel shape, and 500 mL of hexane were added. The sample was left submerged in the solvent for 24 hours, after which the Soxhlet apparatus was operated at 55°C for 24 hours. Upon completion of the extraction process, the product was transferred to a rotary evaporator, and the extract was transferred to a small, sealed container until use in the production

of plastic polymers.

Identification of the components of the hexane extract using gas chromatography-mass spectrometry (GC-MS)

GC-MS was used to identify the components of the extract at the University of Samarra, College of Applied Sciences, using a Shimadzu GCMS-QP2010 Plus instrument manufactured by Shimadzu (Japan). Forty microliters of the extract were taken and diluted to a total volume of 5 mL with ethanol. The injector was set to 2 microliters of the diluted sample using an (Inert Cap 1 capillary column a non-polar column bonded with 100% dimethylpolysiloxane) with a length of 30 meters. The carrier gas was helium at a flow rate of 14.5 mL/min. The oven thermal program began at 60°C with a split ratio of 2:1, and the temperature was held at this level for two minutes. then the temperature was raised at a rate of 30 °C per minute until reaching 180 °C, where it was held for 3 minutes; subsequently, the temperature was raised to 220 °C and maintained for 4 minutes, with a total retention time of 18 minutes. Mass spectra were recorded at an energy of 72 eV and a mass range of 900–500 m/z. The chemical compounds extracted from the sample were identified by comparing the resulting spectra with mass spectra in the libraries available in the instrument software [32].

Production of a Polymer from a Moss Hexane Extract

Diol Reduction

100 mL of the hexane extract was taken, and 10 mL of tetrahydrofuran (THF) and 178 mg of Lithium Aluminum Hydride ($LiAlH_4$) were added to it. The mixture was cooled to 0°C, then heated to boiling for one hour, and left on a stirrer for 3 days at room temperature. The reaction was terminated by adding (2 mL of distilled water and 0.5 mL of 2 M sodium hydroxide solution). The mixture was evaporated at 50°C, and 10 mL of chloroform was added to recrystallize the product.

Polycondensation Reaction

The product prepared in the first reaction was left for one hour, then heated to 80°C, and the temperature was increased by 10°C every 30 minutes until it reached 120°C, after which it was placed on a stirrer for 24 hours. After stirring was complete, 0.1 mL of a solution (0.05 mL of Ti$(OBu)_4$ catalyst in 20 mL of toluene) was added to the resulting mixture, and the temperature was raised to 200 °C for 3 hours [33].

Production of Nanoparticles (Ag NPs, Fe_2O_3 NPs)

10 g of dried algal powder was taken and 100 mL of deionized distilled water was added to it in a 250 mL glass beaker. The mixture was heated to 60°C with magnetic stirring for one hour, after which it was centrifuged at 1000 g for 15 minutes, then filtered using Whatman No. 1 filter paper [28, 34]. Next, 10 mL of the aqueous extract was taken and gradually added to 90 mL of a salt solution containing both silver nitrate ($Ag\ NO_3$) at a concentration of 0.05 M and ferric chloride ($FeCl_3$) at a concentration of 0.1 M (prepared by mixing the metal salt with deionized distilled water) and heated to 40°C under magnetic stirring until the solutions changed color, which is a preliminary indicator of the success of the nanoparticle production process. The solutions were then centrifuged for 15 minutes at 1000 rpm to separate the nanoparticles. The precipitate was washed with deionized water and then with ethanol in a 1: 3, with centrifugation to remove impurities. The precipitate was dried in an oven at 40°C for 12–24 hours to obtain the nanoparticles in powder form. They were stored in opaque containers to protect the silver nanoparticles from light and were characterized using a number of techniques [35].

Characterization of Iron and Silver Nanoparticles

Biologically synthesized iron and silver nanoparticles were characterized using a UV-visible spectrophotometer at wavelengths ranging from (200 to 700 nm), A scanning electron microscope (SEM) was also used to image and determine the size and shape of the iron and silver nanoparticles, in addition to X-ray diffraction (XRD) to determine the crystalline nature of the nanoparticles. Fourier transform infrared (FTIR) spectroscopy was also used, to identify the functional groups that contributed to the preparation of iron and silver nanoparticles [36].

Effect of the Nanocatalyst on the Polymerization Process

To improve the condensation polymerization process and obtain advanced properties for the resulting plastic polymer, the conventional catalyst ($LiAlH_4$) with 0.05 g of a catalyst (ChCl-

based DES/AgNPs catalyst) synthesized from silver nanoparticles (AgNPs), and the nanocatalyst was added to the reaction mixture using ultrasound for 15 minutes prior to addition to ensure its proper distribution [37, 38].

Characterization of the polymer using Fourier Transform Infrared Spectroscopy (FTIR)

The properties of the polymer were characterized at the College of Science, University of Mosul, using a Bruker FTIR spectrometer.

RESULTS AND DISCUSSION

Morphological Diagnosis of the Algae

The sample was Morphologically Diagnosed as shown in Fig. 1 using a light microscope and based on its morphological characteristics through the classification references for algae. It was found that the alga is *Chara vulgaris*, is a green alga.The algae is characterized by a vertical axis attached to the substrate via root-like structures, and a stem consisting of nodes and internodes. From an evolutionary perspective, it is considered a link between algae and bryophytes [39].

Diagnosis of the components of the hexane extract using gas chromatography-mass spectrometry (GC-MS)

GC-MS results in Fig. 2 and Table 1 show that the hexane extract is rich in unsaturated fatty acids such as (linoleic acid)9,12-ctadecadienoic acid (20.39%), which acts as a natural plasticizer, increasing the polymer's flexibility [40]. It also contains long-chain hydrocarbons such as tetracosane and hexadecane, which increase the polymer's hydrophobic properties. Additionally, l-(+)-Ascorbic acid 2,6-dihexadecanoate (29.74%) protects the polymer from thermal degradation

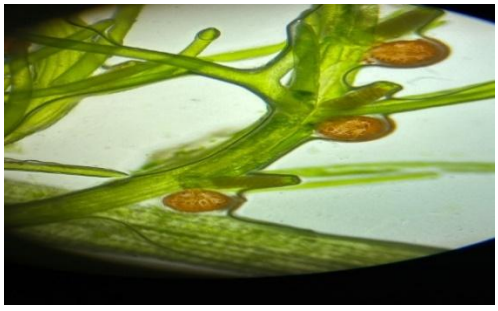

Division: Charophyta, Class: Charophyceae, Order: Charales, Family: Characeae, Genus: *Chara* (Zeneli&Kashta,2016)

Fig. 1. Microscopic image of *Chara vulgaris.*

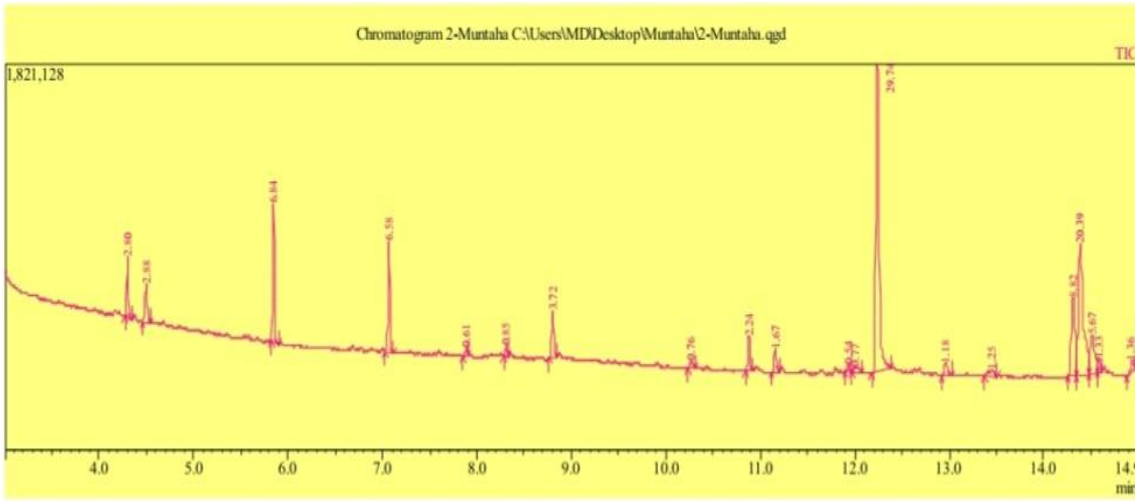

Fig. 2. GC-MS Chromatogram of the hexane extract of *Chara vulgaris*.

during manufacturing [41].

Diagnostic Methods for Iron and Silver Nanoparticles

Color Detection

When the aqueous extract of *Chara* algae was added to both ferric chloride and silver nitrate solutions and mixed thoroughly for 30-45 minutes at 40°C, a color change was observed in each, indicating the production of nanoparticles. The reaction between ferric chloride and the aqueous extract of the algae changed the solution's color

Table 1. Chemical composition and peak area percentages of compounds identified in the *Chara vulgaris* extract by GC-MS analysis.

NO.	Compound Name	Molecular Formula	Peak Area%
1	Tetraethyl silicate	$C_8H_{20}Si$	2.80
2	Undecane	$C_{11}H_{24}$	2.88
3	Dodecane	$C_{12}H_{26}$	6.84
4	Tetradecane	$C14H_{30}$	6.58
5	2(4H) Benzofuranone, 5,6,7,7a-tetrahydro-4,4	$C_{11}H_{16}O_2$	0.61
6	Diethyl Phthalate	$C_{12}H_{14}O4$	0.85
7	Hexadecane	$C_{16}H_{34}$	3.72
8	Tetradecanoic acid	$C_{14}H_{28}O_2$	0.76
9	Heneicosane	$C_{21}H_{44}$	2.24
10	2-Pentadecanone, 6,10,14-trimethyl-	$C_{18}H_{36}O$	1.67
11	Cyclopropanebutanoic acid, 2-[[2-[[2-[(2-pen	$C_{25}H_{42}O_2$	0.54
12	cis-9-Hexadecenoic acid	$C_{16}H_{30}O_2$	0.77
13	l-(+)-Ascorbic acid 2,6-dihexadecanoate	$C_{38}H_{68}O_8$	29.74
14	Tetracosane	$C_{24}H_{50}$	1.18
15	Arachidonic acid	$C_{20}H_{32}O_2$	1.25
16	Phytol, acetate	$C_{22}H_{42}O_2$	8.82
17	9,12-Octadecadienoic acid (Z, Z)-	$C_{18}H_{32}O_2$	20.39
18	cis-10-Heptadecenoic acid	$C_{17}H_{32}O_2$	5.67
19	cis-10-Heptadecenoic acid	$C_{17}H_{32}O_2$	1.33
20	Octadecanoic acid	$C_{18}H_{36}0_2$	1.36

from orange to brown, a preliminary indication of iron ion reduction and the production of iron oxide nanoparticles. Meanwhile, the reaction between the algal extract and silver nitrate changed the solution's color from transparent to purple, confirming the production of silver nanoparticles, as shown in Fig. 3. This color change may be due to the presence of biochemical compounds identified in the *Chara* algal extract Table 1. These active compounds play a significant role in nanoparticle production, as they stabilize and reduce the nanoparticles, allowing for their dispersion and homogeneous distribution in solutions [42, 43].

UV-VIS analysis

The UV of Fe_2O_3NPs in Fig. 4A show the clear absorption edge at wavelength of 350nm These results are consistent with the findings of Subhashini et al. 2018 [44], who reported that the absorption peak of iron oxide nanoparticles lies within the wavelength range of 300-400 nm ,This strong absorption in the UV region is attributed to charge transfer electron transitions, specifically the transfer of electrons from oxygen orbitals (2p)

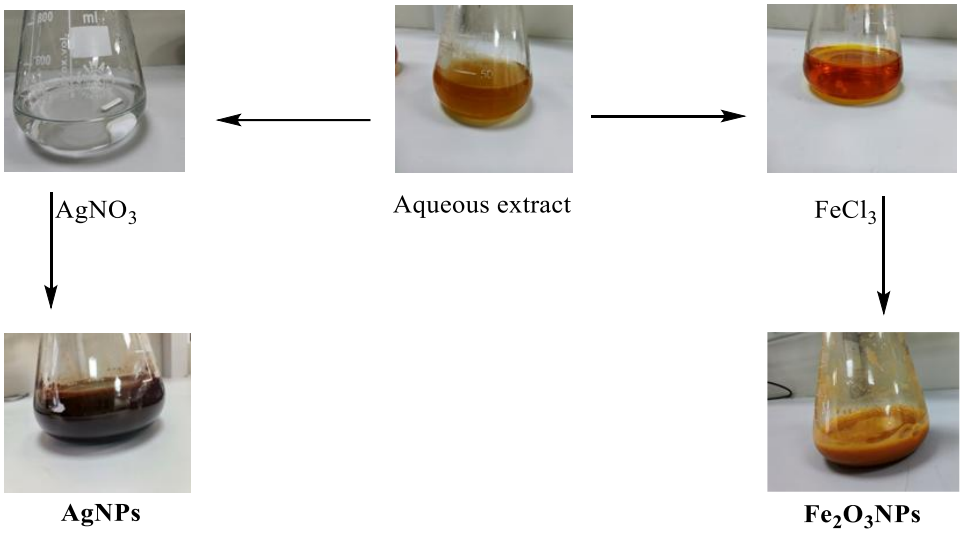

Fig. 3. Color Change in a Solution of Ferric Chloride and Silver Nitrate Using *Chara vulgaris* Extract for the Production of Nanoparticles.

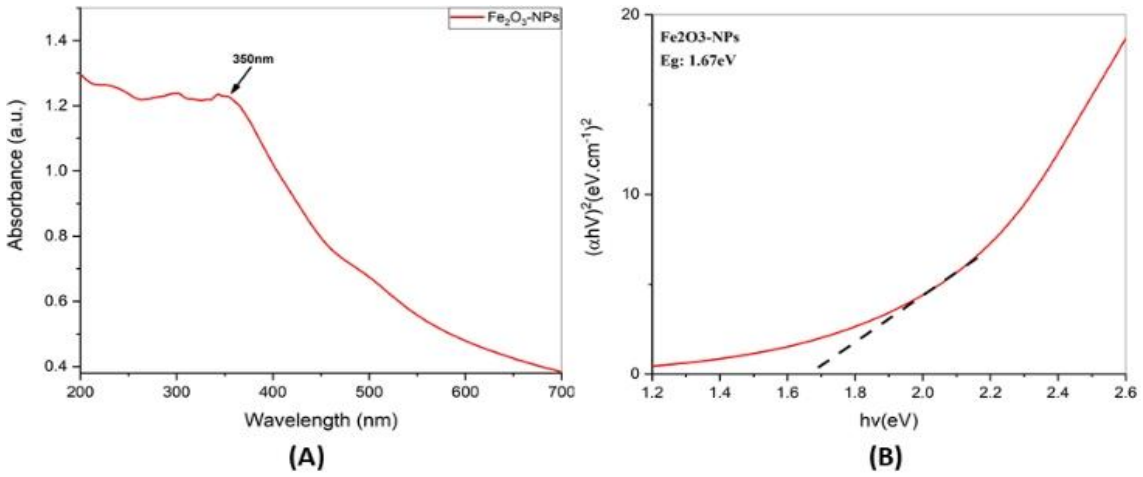

Fig. 4. (A)UV-VIS, (B) Bandgap of Fe_2O_3NPs.

to iron orbitals (3d), that indicate the formation of iron oxide nanoparticle in uniform size.

The optical energy gap was calculating by Tauc's relation by plotting the relationship between $(ahV)^2$ and the photon energy (hv). In Fig. 4B show the energy gap of Fe_2O_3NPs was 1.67 electron volte this result is considered ideal for narrow gap of semi-conductors compared to iron oxide in bulk form. This value reflects the "Quantum Confinement Effect" resulting from reducing the size of the particles to the nanoscale [45, 46].

The curve in Fig. 5A show the clear peak at 450nm, this peak cause by the phenomenon of surface Plasmon resonance which is a collective vibration of free electrons on the surface of silver particles when expose to light. The presence of peak 450nm indicate that the particles are medium in size as a red shift of peak towards

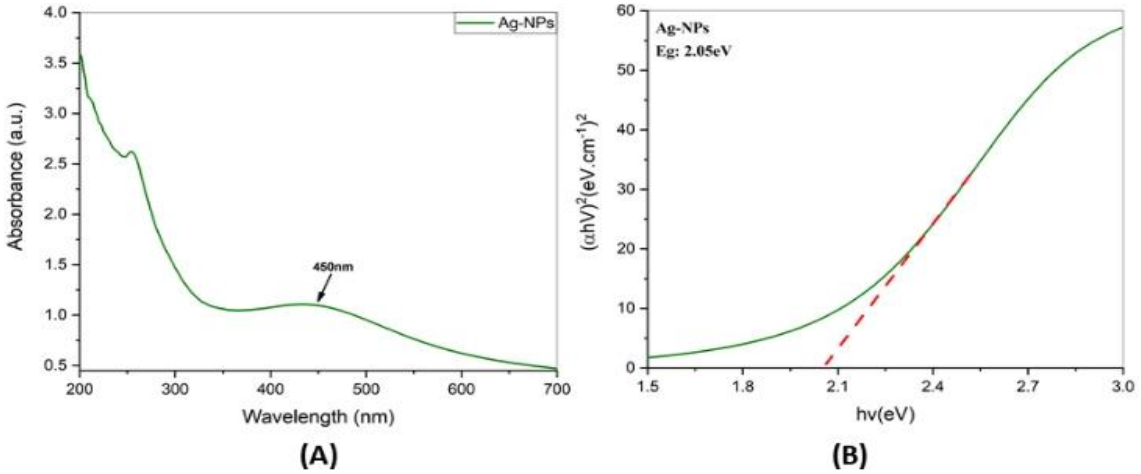

Fig. 5. (A)UV-VIS, (B) Bandgap of AgNPs.

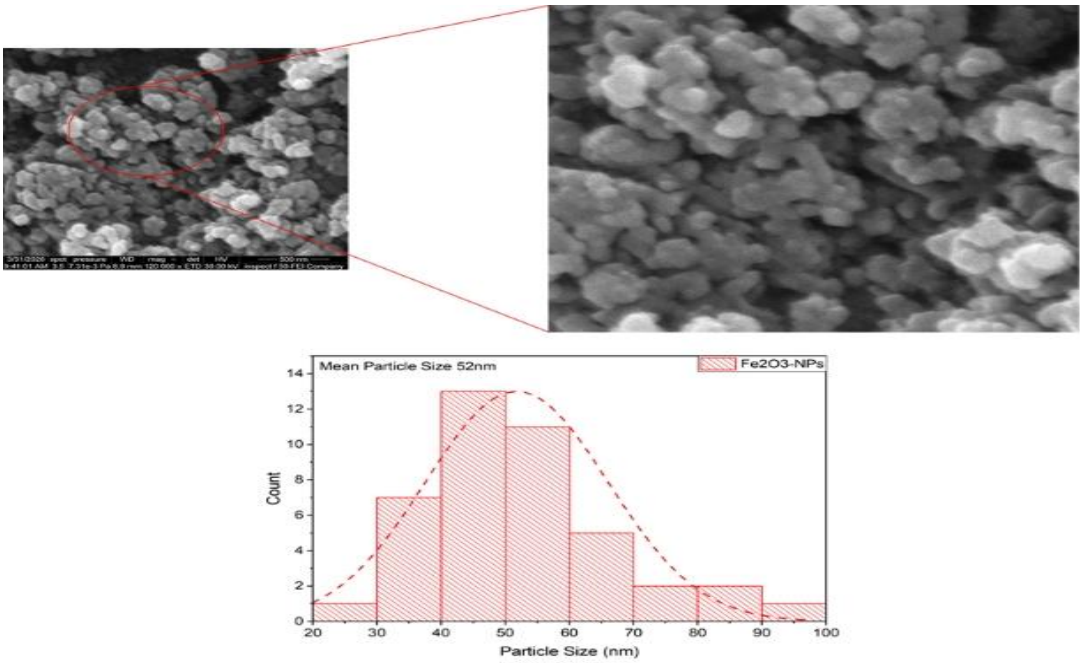

Fig. 6. FESEM of Fe_2O_3NPs.

longer wavelength indicate increase in size, while its presence in this range confirms the successful formation of silver nanoparticles [47]. The energy gap of AgNPs in Fig. 5B was calculating by Tauc's relation by plotting the relationship between $(ahV)^2$ and the photon energy (hv). The energy gap of AgNPs was 2.05ev so this value is low as a compered to bulk silver reflecting the quantum effect and the distinctive optical properties of the prepared nanostructure.

FESEM analysis

The FESEM of Fe_2O_3NPs in Fig. 6 show a structure composed of tightly packed, irregular in shape and it show some aggregation, where the nanoparticles fused together this pattern is very

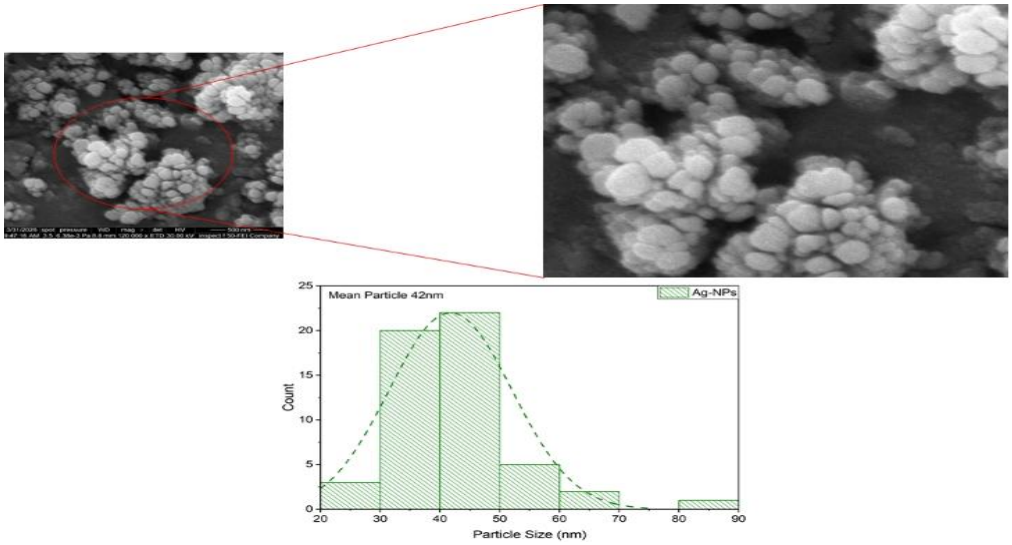

Fig. 7. FESEM of AgNPs.

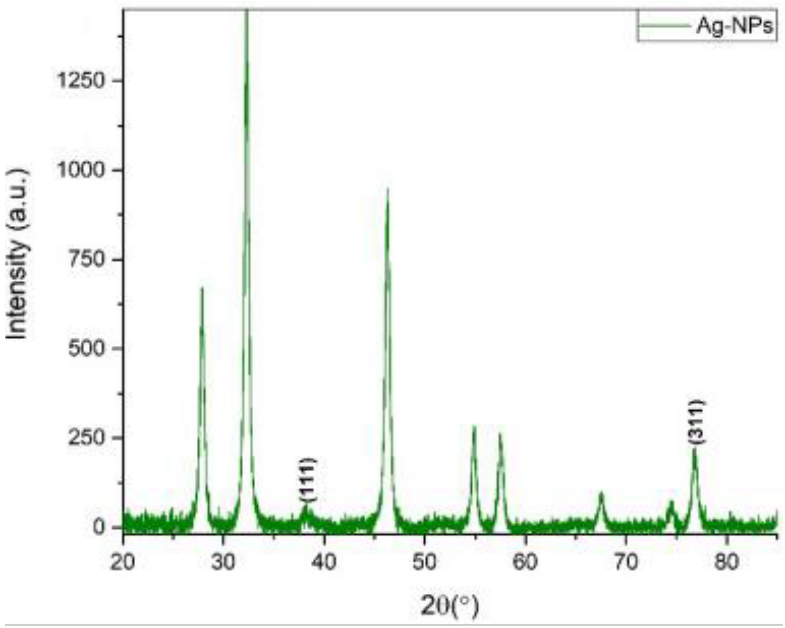

Fig. 8. XRD of Fe_2O_3NPs.

common in nonmetal oxide is often attributed to reaction conditions or the nature of the attraction between the particles. The mean particle size was 52nm, the particles size of nanoparticles is between (20-100) it was within the nanoscale (less than 100nm) which confirms the success of the preparation method [48].

The FESEM of AgNPs in Fig. 7 show the homogenous composition of spherical particles indicating the efficiency of the preparation process in controlling crystal growth. There is a slight tendency for the particles to aggregate

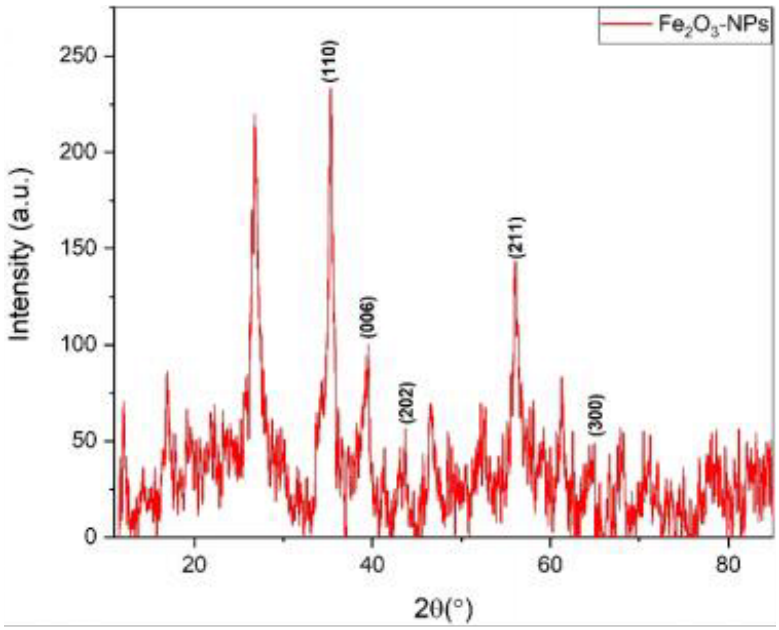

Fig. 9. XRD of AgNPs.

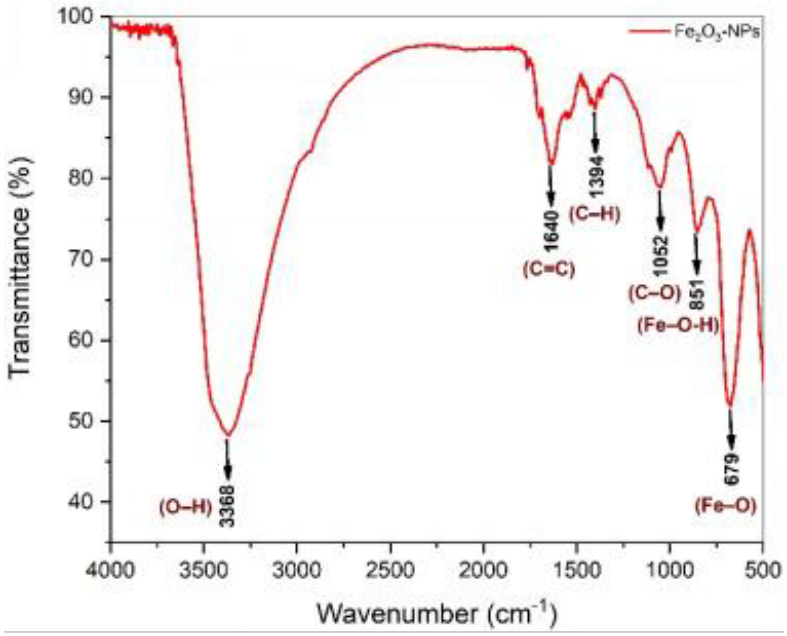

Fig. 10. FTIR of Fe_2O_3NPs.

into clusters, a natural behavior for metallic nanoparticles to reduce their high surface energy. The mean particle size of AgNPs was 41nm, the particale size of nanoparticales is between (20-90) it was within the nanoscale [49].

XRD analysis

The XRD result of Fe_2O_3NPs in Fig. 8 show the hematite phase of Fe_2O_3 with the hexagonal crystal system. All the diffraction peaks at levels (110), (006), (202), (211) and (300) matching with

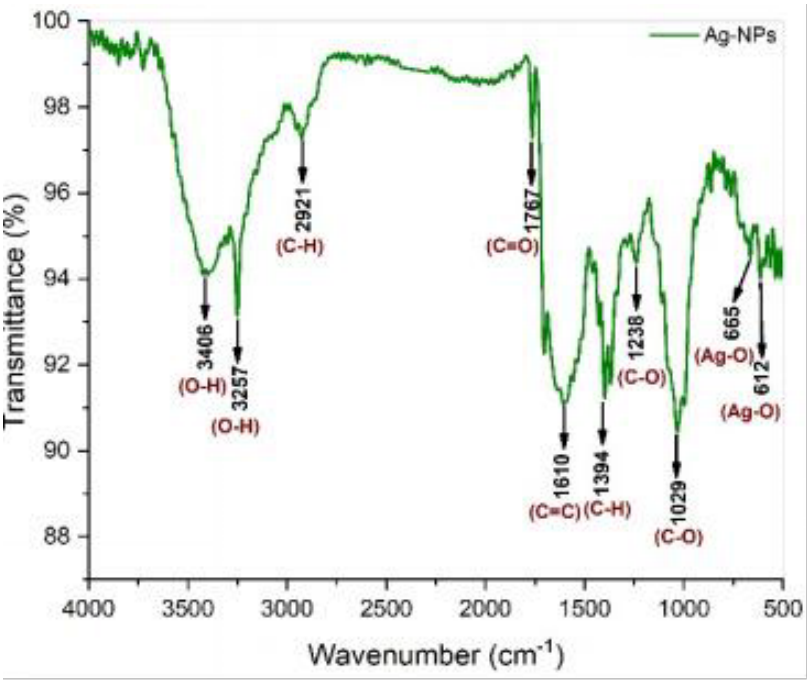

Fig. 11. FTIR of AgNPs.

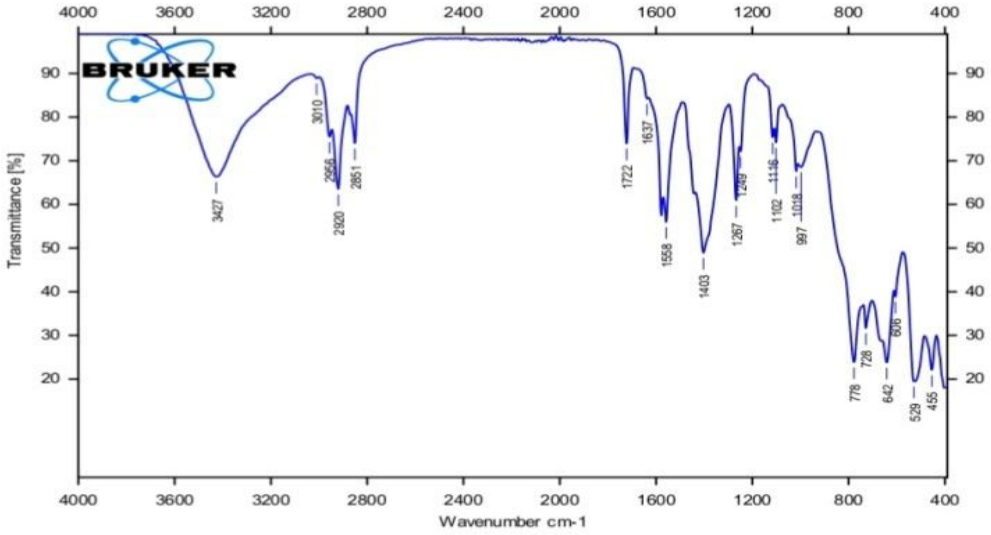

Fig. 12. FTIR Of catalyst-produced polymer (Ti(OBu).

JCPDS card 33-0664. The display of the peaks also confirmed the nanoscale nature of the material, with the pattern being free of any peaks belonging to impurities, indicating the success of the preparation process and the acquisition of a pure and stable phase [50]. Fig. 9 shows the XRD analysis of AgNPs that show the distance bands at specific diffraction angles corresponding to the (111) and (311) which are matching to JCPDS card 04-0783. The silver nanoparticles have a face centered cubic crystal structure. While the secondary peaks attributed to the organic materials of algae extract use in reduction and precipitation process [51, 52].

FTIR analysis

The FTIR analysis of Fe_2O_3NPs in Fig. 10 shows that the spectrum conforms the formation of iron oxide mineral network and the presence stabilizing functional groups the 676 peak is the important peak and represent the stretch vibration of the (Fe-O) bond. The 851 peak this is due to the bending vibration of (Fe-O-H) bond appear as a result of the interaction of particle surface with moisture or hydroxyl groups. The bond (1052) represents the stretch vibration of the (C–O) bond, resulting from the residue of organic compounds that coated the iron oxide during preparation. The bond (1394): is due to the bending vibrations of the (C–H) bonds or carboxyl groups. The bond (1640): represents the (C=O) or (C=C) vibrations; these bonds play a role in binding the nanoparticles to the catalysts in the extract. The broad bond (3368): a strong, broad peak due to the stretch vibration of the hydroxyl group (O–H), indicating the presence of water molecules adsorbed on the oxide surface or strong hydrogen bonds [50, 53]. Fig. 11 shows the FTIR analysis of AgNPs, this spectrum is considered evidence of a bio capsulation process where the bands resulting from the plant extract that coated the silver atoms are visible. The bands in 3406, 3257 are responsible for reducing silver ions from (Ag+) to (Ag0), band in 2921 represent the stretch vibration of an aliphatic bond indicate of carbon chain from the extract biomolecules. Bond (1767) is a sharp bond belonging to the carbonyl group (C=O), indicating the presence of esters or organic acids that increase the stability of the particles. Bond (1610) is due to aromatic (C=C) bonds or protein vibrations (Amide I), confirming the presence of a protein layer that protects the particles from agglomeration. Bonds (1238 and 1029) are due to stretch vibrations of the (C–O) bond, indicating the presence of alcohols and carbohydrates from the extract acting as surface

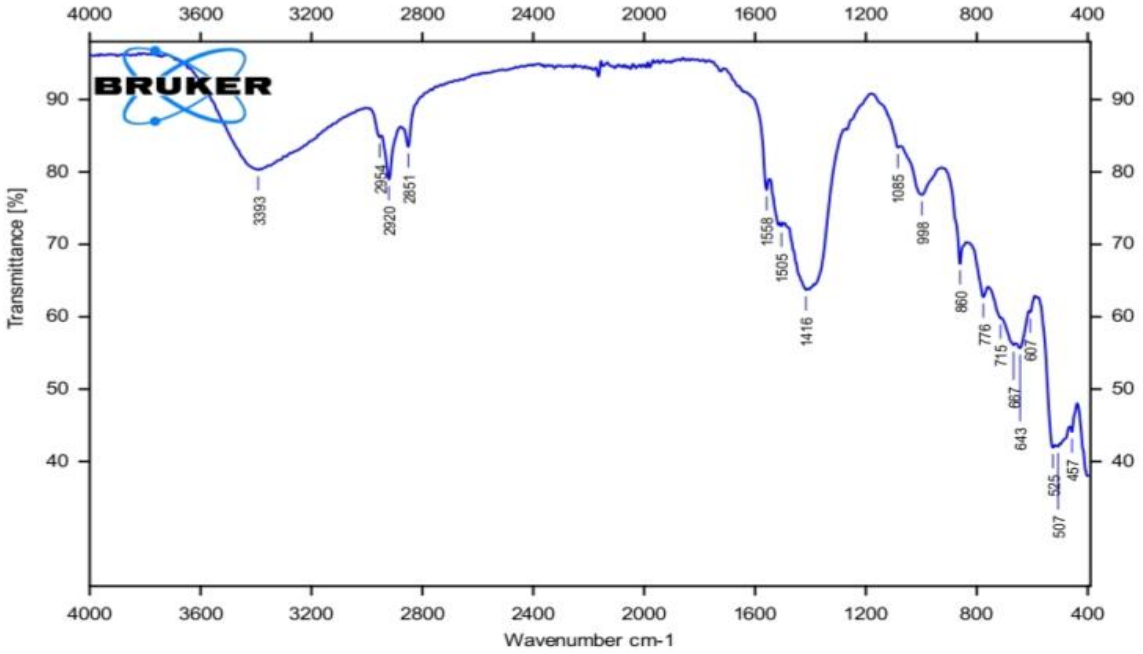

Fig. 13. FTIR of catalyst-produced polymer ChCl-based DES/AgNPs.

stabilizers. Loose bonds (665 and 612) indicate the interaction between the silver surface and the surrounding organic groups [54].

FTIR Polymer Diagnostics

The results in Fig. 12 confirm the success of the polymerization process using the catalyst (Ti $(OBu)_4$), as evidenced by the appearance of several absorption bands, including the 1722 cm^{-1}. This band is attributed to the carbonyl group C=O, which is a product of the polymerization of the organic bonds in the extract, in addition to the C-O bonds in the 1000–1300 cm^{-1} range for ester compounds, and the presence of bands resulting from the vibration of the C-H bond at (2851–2920 cm^{-1}), which contributes to the increased hydrophobicity of the resulting polymer. The broad band at 3427 cm^{-1} is attributed to the vibration of the hydroxyl group (OH), which provides sites for enzymatic and microbial activity [55]. The appearance of C=C bond peaks at 1637 cm^{-1} and at 3010 cm^{-1} for the C=C-H bond indicates that the polymer retains a proportion of unsaturated bonds, which are flexible, slip-pronechains.

The spectrum shown in Fig. 13 reveals the nano-catalyzed polymer compound, where a broad band appears at 3393 cm^{-1}; the reason for its broadening compared to the initial spectrum is the formation of a network of hydrogen bonds between the active surface of the high-energy nano-catalyst and the active groups of the polymer. The absence of the C=O carbonyl peak at 1722 cm^{-1} was observed, along with the appearance of a peak at 1416 cm^{-1} accompanied by overlapping peaks (1505–1558 cm^{-1}). This is attributed to the participation of the oxygen double bonds in the carbonyl group in stabilizing and confining the nanoparticles, as well as the appearance of new, sharp absorption peaks at the low-frequency ranges of 643 cm^{-1} and 525 cm^{-1} 507 cm^{-1} and 427 cm -1 are attributed to oxygen–metal bond vibrations (Ag–O), which strongly indicates the incorporation of the nanocatalyst into the biopolymer [56].

CONCLUSION

The results indicated the successful green and sustainable synthesis of iron oxide (Fe_2O_3NPs) and silver nanoparticles (Ag NPs) using the aqueous algal extract. Furthermore, the efficiency of their incorporation and stabilization within the biopolymer prepared from the hexane extract, characterized by its content of active compounds and fatty acids, was demonstrated. Colorimetric tests and comparisons of the secondary particles confirmed a color change, an important physical indicator proving the reduction of metal ions and their transformation into stable secondary particles. UV-Vis spectroscopy results confirmed the successful reduction and formation of nanoparticles, a clear absorption edge for iron oxide appeared at 350 nm with an energy gap of 1.6 ev while the surface plasmon resonance peak for silver appeared at 450 nm with an energy gap of 2.05 ev. FTIR spectroscopy results reinforced this conclusion by showing the role of the extract's organic compounds (such as carbohydrates, proteins, and carbonyl bonds) as reducing agents and surface stabilizers that coated the nanoparticle and prevented random aggregation. X-ray diffraction (XRD) results confirmed the high purity and stable precipitation of the prepared crystalline phases without the appearance of impurities. The formation of the hematite phase with the hexagonal crystal system and the iron oxide particles with the face-centered cubic crystal structure of the silver nanoparticles was confirmed. Scanning electron microscopy (FESEM) images revealed that the iron oxide particles possess a tightly packed and irregularly shaped structure with an average particle size of 52, while the silver particles exhibited normal behavior to reduce their high surface energy with an average size of 41, confirming the success of the preparation method in obtaining ideal nanoscale sizes. In addition, spectroscopic examinations proved the success of the polymerization process using the catalyst (Ti $(OB)_4$) and the formation of ester chains. When the nanoparticles were incorporated into the biopolymer, the FTIR spectrum showed a broadening and shift in the hydroxyl bond band, indicating the formation of a strong, interlocking hydrogen bond network between the polymer's active groups and the active surface of the nano catalyst. This was supported by the emergence of new, sharp vibrations of the oxygen-metal (Ag-O) bond, demonstrating the achievement of efficient physical and chemical integration and stabilization of the nanoparticles within the prepared biopolymer network in a shorter time. Also, the ChCl-based DES/AgNPs catalyst gave excellent results compared to the first catalyst, confirming the superiority of green synthesis of silver nanoparticles synthesized from algal extract.

CONFLICT OF INTEREST

The authors declare that there is no conflict of interests regarding the publication of this manuscript.

REFERENCES

1. Arora Y, Sharma S, Sharma V. Microalgae in Bioplastic Production: A Comprehensive Review. Arabian Journal for Science and Engineering. 2023;48(6):7225-7241.
2. Park YK, Chin Y-W. Degradation of Bisphenol A by Bacillus subtilis P74 Isolated from Traditional Fermented Soybean Foods. Microorganisms. 2023;11(9):2132.
3. Saleh H, Al-Kahlidi M, Abulridha H, Banoon S, Abdelzaher M. Current Situation and Future Prospects for Plastic Waste in Maysan Governorate: Effects and Treatment During the COVID-19 Pandemic. Egyptian Journal of Chemistry. 2021;64(8):4449-4460.
4. Al-Sulami A, Al-Taee A. Potability of Drinking Water in Basra-Iraq. Tigris and Euphrates Rivers: Their Environment from Headwaters to Mouth: Springer International Publishing; 2021. p. 541-552. http://dx.doi.org/10.1007/978-3-030-57570-0_23
5. Hassan S, Al_Ezee AMM, Al Sulivany BSA, Hassan NE. Evaluating the Ecological Consequences of Heavy Metals Contamination on Aquatic Ecosystem Functioning in the Tigris River, Iraq. Egyptian Journal of Aquatic Biology and Fisheries. 2026;30(2):191-202.
6. Alshahri M, Al-Mashhadany M. Evaluation of Surface Water Quality for Aquatic Life Using Artificial Intelligence Method. Egyptian Journal of Aquatic Biology and Fisheries. 2025;29(1):2879-2892.
7. Sofo A, Elshafie HS, Camele I. Structural and Functional Organization of the Root System: A Comparative Study on Five Plant Species. Plants. 2020;9(10):1338.
8. Üstün R, Amjid M. Assessment of Germination and Seedling Development Factors of Soybean Cultivars in Different Salinity Levels. Black Sea Journal of Agriculture. 2024;7(5):477-485.
9. Sahira K, Al-Abboodi AK. Parasitological Contamination of Raw Vegetables collected from selected Local Markets in Maysan Province, South of Iraq. Nigerian Journal of Parasitology. 2023;44(2):464-473.
10. Faiq NH, Ahmed ME. Effect of Biosynthesized Zinc oxide Nanoparticles on Phenotypic and Genotypic Biofilm Formation of Proteus mirabilis. Baghdad Science Journal. 2024;21(3):0894.
11. Al-Abboodi A, Mhouse Alsaady HA, Banoon SR, Al-Saady M. Conjugation strategies on functionalized iron oxide nanoparticles as a malaria vaccine delivery system. Bionatura. 2021;3(3):2009-2016.
12. Review for "Anti-obesity effect of unsaponifiable matter from hemp seed in 3T3-L1 adipocytes and high-fat diet-induced obese mice". Royal Society of Chemistry (RSC); 2025.
13. Zainab JM, Sahira K, Al-Abboodi AK, Alsaady HA. Enhancing Pediculicidal Activity Against Pediculus humanus capitis Using Iron Oxide Nanoparticle-Based Formulations of some Plant Extracts and Acetic Acid Solution. Nigerian Journal of Parasitology. 2024;45(2):460-469.
14. Al-Abboodi A, Falih IQ, Al-Asadi M, Hussein BA, Al-Saady MAAJ, Abdullah TA, et al. Iron-oxide nanoparticles (SPIONs) enhance malaria vaccine antibody response. Vaccine. 2026;77:128353.
15. Jabber Al-Saady MAA, Aldujaili NH, Rabeea Banoon S, Al-Abboodi A. Antimicrobial properties of nanoparticles in biofilms. Bionatura. 2022;7(4):1-9.
16. Banoon SR, Ghasemian A. The Characters of Graphene Oxide Nanoparticles and Doxorubicin Against HCT-116 Colorectal Cancer Cells In Vitro. J Gastrointest Cancer. 2021;53(2):410-414.
17. Aldujaili NH, Banoon SR. ANTIBACTERIAL CHARACTERIZATION OF TITANIUM NANOPARTICLES NANOSYNTHESIZED BY STREPTOCOCCUS THERMOPHILUS. Periódico Tchê Química. 2020;17(34):311-320.
18. AlHasan L, Qi A, Al-Aboodi A, Rezk A, Shilton RR, Chan PPY, et al. Surface acoustic streaming in microfluidic system for rapid multicellular tumor spheroids generation. SPIE Proceedings; 2013/12/07: SPIE; 2013. p. 89235C.
19. Al-Abboodi A, Tjeung R, Doran P, Yeo L, Friend J, Chan P. Microfluidic chip containing porous gradient for chemotaxis study. SPIE Proceedings; 2011/12/21: SPIE; 2011. p. 82041H.
20. Al-Abboodi A, Tjeung R, Doran PM, Yeo LY, Friend J, Yik Chan PP. In Situ Generation of Tunable Porosity Gradients in Hydrogel-Based Scaffolds for Microfluidic Cell Culture. Advanced Healthcare Materials. 2014;3(10):1655-1670.
21. Behera M, Behera PR, Bhuyan PP, Singh L, Pradhan B. Algal Nanoparticles and Their Antibacterial Activity: Current Research Status and Future Prospectives. Drugs and Drug Candidates. 2023;2(3):554-570.
22. Rahim Hateet R, Alag Hassan Z, Abdullah Al-Mussawi A, Rabeea Banoon S. Optimization of cultural conditions affecting improved bioactive metabolite production by endophytic fungus Trichoderma harzianum. Bionatura. 2021;6(4):2187-2192.
23. Omar ST, Ali WK. Effects of Zinc Oxide Nanoparticles (ZnO NPs) Synthesized from River Oak Casuarina cunninghamiana Miq.,1848 Leaf Extracts on Three Insects Species. Iraqi Journal of Science. 2024:6946-6958.
24. Vetchinkina E, Loshchinina E, Kupryashina M, Burov A, Pylaev T, Nikitina V. Green synthesis of nanoparticles with extracellular and intracellular extracts of basidiomycetes. PeerJ. 2018;6:e5237.
25. Joudeh N, Linke D. Nanoparticle classification, physicochemical properties, characterization, and applications: a comprehensive review for biologists. Journal of Nanobiotechnology. 2022;20(1).
26. Yaseen SN, Al-Fakhry HH, Saleh MY. Local Rosuvastatin Loaded by Thiolated Hyaluronan Hydrogel for Post orthodontic Relapse Reduction. In Vitro Preparation and In Vivo Assessment in Rabbit. Egyptian Journal of Veterinary Sciences. 2025;56(7):1647-1659.
27. Madhiyazhagan P, Murugan K, Kumar AN, Nataraj T, Subramaniam J, Chandramohan B, et al. One pot synthesis of silver nanocrystals using the seaweed Gracilaria edulis: biophysical characterization and potential against the filariasis vector Culex quinquefasciatus and the midge Chironomus circumdatus. J Appl Phycol. 2016;29(1):649-659.
28. Hassan KT, Ibraheem IJ, Hassan OM, Obaid AS, Ali HH, Salih TA, et al. Facile green synthesis of Ag/AgCl nanoparticles derived from Chara algae extract and evaluating their antibacterial activity and synergistic effect with antibiotics. Journal of Environmental Chemical Engineering.

2021;9(4):105359.
29. Mahajan P, Kaushal J, Upmanyu A, Bhatti J. Assessment of Phytoremediation Potential of Chara vulgaris to Treat Toxic Pollutants of Textile Effluent. J Toxicol. 2019;2019:1-11.
30. Taleei MM, Karbalaei Ghomi N, Jozi SA. Arsenic Removal of Contaminated Soils by Phytoremediation of Vetiver Grass, Chara Algae and Water Hyacinth. Bulletin of Environmental Contamination and Toxicology. 2018;102(1):134-139.
31. Verawaty M, Melwita E, Apsari P, Wiyahsari M. Cultivation Strategy for Freshwater Macro- and Micro-Algae as Biomass Stock for Lipid Production. Journal of Engineering and Technological Sciences. 2017;49(2):261-274.
32. Meyer MR. Hans-Joachim Hübschmann: Handbook of GC-MS: fundamentals and applications, 3rd ed. Analytical and Bioanalytical Chemistry. 2016;408(6):1535-1536.
33. Roesle P, Stempfle F, Hess SK, Zimmerer J, Río Bártulos C, Lepetit B, et al. Synthetic Polyester from Algae Oil. Angew Chem Int Ed. 2014;53(26):6800-6804.
34. Hassan EM, Saleh MY, Saied SM, Kazemi M. Magnetic-MOF Zinc nanocatalyst in DESs Solvent: a sustainable route for 2,4-Disubstituted Quinoline synthesis. J Organomet Chem. 2025;1040:123812.
35. Kalel R. Silica Immobilized Brønsted-Lewis Acidic Ionic Liquid : Heterogeneous catalyst for Condensation-Aromatization in the Synthesis of 2-(4-nitrophenyl)-1H-benzimidazole by cooperative catalysis. Peeref; 2023 2023/03/21.
36. Mohammad MK, Ahmed SH, Hameed RS, Al-Kharkhi IHT. Synthesis Characterization of new Nanoparticles Derived From Iron Oxide and Beta vulgaris extracts and its Bioactivity against Pantoea spp. Indian Journal of Forensic Medicine and Toxicology. 2019;13(4):362.
37. Rozilah A, Jaafar CNA, Sapuan SM, Zainol I, Ilyas RA. The Effects of Silver Nanoparticles Compositions on the Mechanical, Physiochemical, Antibacterial, and Morphology Properties of Sugar Palm Starch Biocomposites for Antibacterial Coating. Polymers. 2020;12(11):2605.
38. Assad H, Fatma I, Kumar A. Ionic Liquid in Phase Transfer Catalysis. Ionic Liquids: Eco-friendly Substitutes for Surface and Interface Applications: BENTHAM SCIENCE PUBLISHERS; 2023. p. 302-325.
39. Abass MH, Al-Utbi SD, Al-Samir EAH. Morphological and biochemical impact of different decontamination agents on date palm (Phoenix dactylifera L.) procallus. Australian Journal of Crop Science. 2016;10(07):1022-1029.
40. Vieira MGA, da Silva MA, dos Santos LO, Beppu MM. Natural-based plasticizers and biopolymer films: A review. Eur Polym J. 2011;47(3):254-263.
41. Gupta RK, Manisha, Ali EAE, Areekal NN, Patel J, Pipliya S, et al. Vitamin C-infused biopolymer films: a multifunctional approach for active food packaging and preservation. Sustainable Food Technology. 2026;4(1):25-50.
42. Buarki F, AbuHassan H, Al Hannan F, Henari FZ. Green Synthesis of Iron Oxide Nanoparticles Using Hibiscus rosa sinensis Flowers and Their Antibacterial Activity. Journal of Nanotechnology. 2022;2022:1-6.
43. Sustainable Synthesis of Ionic Liquid-Functionalized Zinc Oxide Nanosheets (IL@ZnO): Evaluation of Antibacterial Potential Activity for Biomedical Applications. American Chemical Society (ACS). http://dx.doi.org/10.1021/acsabm.1c01258.s001
44. Subhashini R, Arjunan S. Synthesis and physicochemical properties of bis(l-asparaginato) zinc(II): A promising new semiorganic crystal with high laser damage threshold for shorter wavelength generation. Optics and Laser Technology. 2018;101:248-256.
45. Hamid Al-Sultan RM, Abdulsalaam Al-Sultan A, Hayawi MA, Aldahham BJM, Saleh MY, Mohammed HA. The effect of subclinical thyroid dysfunction on B- type natriuretic peptide level. Bionatura. 2022;7(2):1-9.
46. Tabassum N, Singh V, Chaturvedi VK, Vamanu E, Singh MP. A Facile Synthesis of Flower-like Iron Oxide Nanoparticles and Its Efficacy Measurements for Antibacterial, Cytotoxicity and Antioxidant Activity. Pharmaceutics. 2023;15(6):1726.
47. Kumar B, Smita K, Cumbal L, Debut A. Green synthesis of silver nanoparticles using Andean blackberry fruit extract. Saudi J Biol Sci. 2017;24(1):45-50.
48. Hasan SJ, Evan TS, Rana OM, Iman HH, Subash CBG. A Study on Different Au Concentrations for A-Fe_2O_3@Au Hybrid Structure Preparation and Characterization. International Journal of Nanoelectronics and Materials (IJNeaM). 2025;18(June):139-152.
49. Ghasemi M, Govahi M, Litkohi HR. Green synthesis of silver nanoparticles (AgNPs) and chitosan-coated silver nanoparticles (CS-AgNPs) using Ferula gummosa Boiss. gum extract: A green nano drug for potential applications in medicine. Int J Biol Macromol. 2025;291:138619.
50. Al-assdy HQ, Al-Tamimi WH, Almansoory AF. Treatment Wastewater of Oil Refinery by Fe_2O_3 NPs produce by the novel Alishewanella Jeotgali strain HAQ8. Karbala International Journal of Modern Science. 2025;11(2).
51. Fernandes Júnior EL, Maria de Melo Amaral I, de Lima GT, da Silva RE, Nobre ARdA, Raimundo RA, et al. Biosynthesis of Silver Nanoparticles from Hybrid Polymer: Characterization, Approach from XRD and Investigation of Antimicrobial Activity. ACS Omega. 2026;11(15):22918-22928.
52. Thamer H, Saleh M. Catalyst-Free Synthesis of Polyheterocyclic Compounds via Ugi Reactions: Structural Elucidation and Antileishmanial Screening Using Promastigote Viability Assay. Tropical Journal of Natural Product Research. 2026;10(2):7150-7155.
53. Ali AH, Saleh MY, Yaqoob QA, Saied SM, Hasan MS, Owaid KA, et al. Comprehensive evaluation of antibacterial and anticancer activities from indole butanoic acid. Journal of Genetic Engineering and Biotechnology. 2025;23(1):100452.
54. Lasmi F, Hamitouche H, Laribi-Habchi H, Benguerba Y, Chafai N. Silver Nanoparticles (AgNPs), Methods of Synthesis, Characterization, and Their Application: A Review. Plasmonics. 2025;20(11):9455-9488.
55. Vajanapanich P, Nearmnala P, Parkbhorn J, Nutho B, Rungrotmongkol T, Hongdilokkul N. Catalytic Residue Reprogramming Enhances Enzyme Activity at Alkaline pH via Phenolate-Mediated Proton Transfer. ACS Synthetic Biology. 2025;14(9):3612-3623.
56. Saini S, Saini T, Verma V, Meena J. Studies on biopolymer -Based Nanocomposites reinforced with metallic Nanoparticles. Acta Biology Forum. 2024;4(2):6-15.